Inorganic Chemistry

pubs.acs.org/IC

Article

Cyclometalated Iridium(III) Complexes as High-Sensitivity Two-Photon Excited Mitochondria Dyes and Near-Infrared Photodynamic Therapy Agents

Xu-Dan Bi, Rong Yang, Yue-Chen Zhou, Daomei Chen, Guo-Kui Li, Yuan-Xiao Guo, Meng-Fan Wang, Dandan Liu,* and Feng Gao*

Cite This: https://dx.doi.org/10.1021/acs.inorgchem.0c01509

Read Online

ACCESS | Metrics & More | Article Recommendations | Supporting Information

ABSTRACT: Photodynamic therapy (PDT) using two-photon near-infrared light excitation is a very effective way to avoid the use of short-wavelength ultraviolet or visible light which cannot efficiently penetrate into the biological tissues and is harmful to the healthy cells. Herein, a series of cyclometalated Ir(III) complexes with a structurally simple diimine ligand were designed and the synthetic route and preparation procedure were optimized, so that the complexes could be obtained in apparently higher yield, productivity, and efficiency in comparison to the traditional methods. Their ground state and excited singlet and triplet state properties were studied by spectroscopy and quantum chemistry theoretical calculations to investigate the effect of substituent groups on the photophysical properties of the complexes. The Ir(III) complexes, especially **Ir1** and **Ir3**, showed very low dark toxicities and high phototoxicities under both one-photon and two-photon excitation, indicating their great potential as PDT agents. They were also found to be highly sensitive two-photon mitochondria dyes.

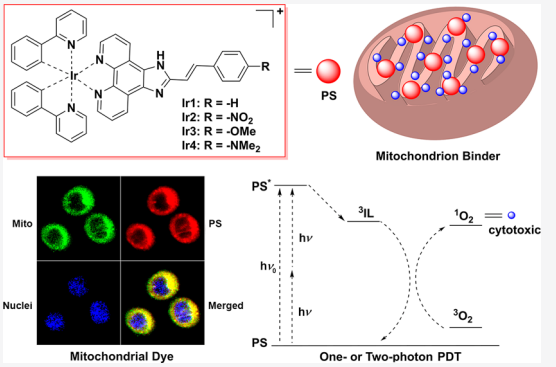

INTRODUCTION

Photodynamic therapy (PDT) is a minimally invasive treatment approved for the treatment of cancerous tumors and of noncancerous diseases, involving the interaction of the photosensitizer (PS), light component, and molecular oxygen.[1−3] The vast majority of current PSs clinically approved for PDT are activated by short-wavelength ultraviolet (UV) or visible (Vis) light, which cannot efficiently penetrate into the biological tissues, and PDT modality is restricted to the treatment for superficial lesions.[4] Notably, near-infrared (NIR) light in the range of around 700−1000 nm, known as the "biological transparency window", displays minimum photodamage to healthy cells, reduced scattering from tissue components, and better tissue penetration (e.g., <10 cm) than UV or Vis light (e.g., <1 cm).[5] Therefore, more attention has recently focused on shifting the excitation wavelength to the NIR region for deep PDT treatment.

One approach to reach the NIR region relies on organic PSs, such as derivatives of boron dipyrromethene (BODIPY), porphyrin, and phthalocyanine that absorb in the 650−750 nm region.[6] Another choice is upconverting nanoparticles (UCNPs), a class of nanoparticles that emit UV or Vis light under NIR light excitation.[7−9] More recently, PSs with two-photon (TP) absorption properties have attracted a great deal of attention in PDT.[10−12] The TP-PDT agent molecule is promoted to an excited state, the same PS-active excited state as for one higher-energy photon excitation, by the simultaneous absorption of two lower-energy NIR photons, each of which contributes half of the total energy required to induce emission. In comparison with traditional one-photon (OP) PDT agents, TP-PDT agents require the application of a low-energy NIR laser as a light source, which gives a possibility of higher light dose administration and minimizes the side effects thanks to the reduced interaction between the NIR light and the tissue.[13]

Metal-containing PSs have emerged as promising PDT systems because of their rich photochemical and photophysical properties derived from various excited-state electronic configurations.[12,14−17] On one hand, their energy- and electron-transfer processes can yield highly potent oxygen-dependent and/or oxygen-independent photobiological activity.[18] On the other hand, the large quantum yields for triplet-state formation and the characteristic reactivities of the different excited-state configurations offer the opportunity to

Received: May 23, 2020

rationally design transition-metal complexes with desirable photobiological mechanisms that are simply not possible with organic PSs.

In 2014, You and Nam synthesized the first Ir(III)-based molecular dyad (Irbtp−RhB) capable of lysosomal staining, $^1O_2$ sensitization, and TP-PDT (Figure 1).[19] Lemercier and

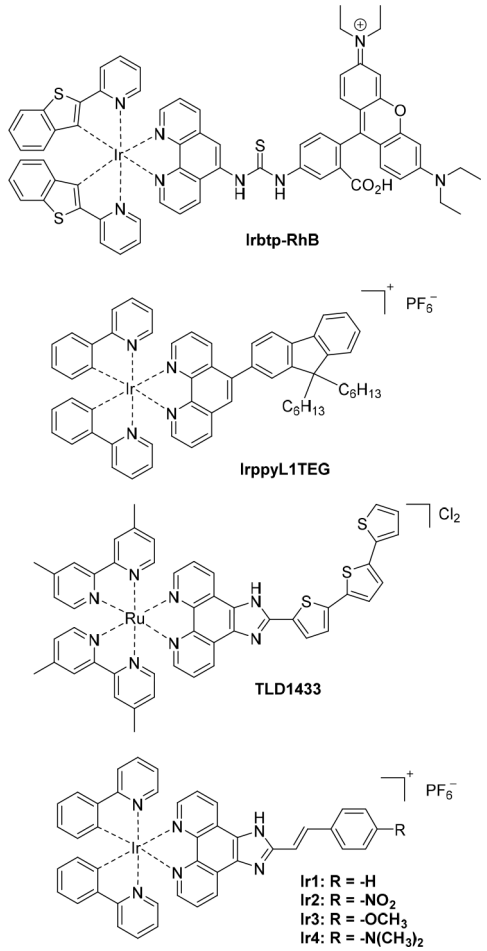

Figure 1. Representive metal complexes for PDT and complexes **Ir1**−**Ir4** designed in this study.

Natrajan also developed a cyclometalated Ir(III) complex (Figure 1) as a PS for TP-PDT using the ligand of RuL1TEG, the first Ru(II) complex as a PS for TP-PDT.[20,21] Since then, luminescent cyclometalated Ir(III) complexes with TP absorption behavior have been widely investigated, and their targets in tumor cells have been reported to be DNA, intracellular nucleus, endoplasmic reticulum, lysosome, mitochondria, cytoplasm, peptide, and protein.[12,22−24] In comparison to Ru(II) complexes, Ir(III) complexes have higher ligand field strength and stronger spin−orbital coupling provided by the third-row transition metal. Furthermore, heteroleptic Ir(III) complexes with bipyridyl (N^N) and cyclometalating (C^N) ligands have shown high photostability due to high-lying metal-centered states and easily tunable highest occupied molecular orbital (HOMO) and lowest unoccupied molecular orbital (LUMO) energy levels. Their high photostability allows cyclometalated Ir(III) complexes to be used for continuous irradiation and real-time monitoring of intracellular trafficking.[25] Their long-lived triplet states result in long lifetimes and facilitate possible reactions with oxygen to generate singlet oxygen ($^1O_2$) and/or other reactive oxygen species (ROS), and their large Stokes shift can minimize the possible self-quenching effect even at high concentration.[26−29] In addition to d-block metals, f-block-element complexes, particularly Gd(III) and Lu(III), have also been reported for their TP-PDT activity.[30,31]

It is encouraging that, after years of efforts, TLD1433 became the first Ru(II)-based PS that entered a human clinical trial (ClinicalTrials.gov, identifier NCT03053635) for non-muscle invasive bladder cancer in 2018. As summarized in the recent review by McFarland,[32] the developer of TLD1433, an ideal PDT agent should meet the following standards: (1) effective generation of cytotoxic $^1O_2$ and/or other ROS, (2) large molar extinction coefficient in the PDT window, (3) preferential tumor accumulation and rapid systemic clearance, (4) amphiphilic structure, (5) no dark toxicity, (6) chemical stability, (7) solubility in injectable formulations, and (8) chemically pure and easy to obtain via high-yielding reactions.[33] This last standard concerning preparation has been placed in an unimportant position in the pursuit of high activity. Almost all reported Ir(III)-based PDT agents have complex ligand structures that are difficult to synthesize, and the amount of preparation is usually in milligrams. This is undoubtedly an obstacle for further *in vivo* experiments and clinical research.

Overall, compounds with a high $^1O_2$ yield upon NIR irradiation and a simple chemical structure will be the ideal choice for PDT. Therefore, the focus of this study is to introduce structurally simple functional groups which are beneficial to the production of $^1O_2$ into Ir(III) complexes which have been proven to have good TP-PDT properties. Cinnamaldehyde, as an active compound isolated from the traditional medicinal herb *Cinnamomum cassia*, has been reported to induce a ROS-mediated mitochondrial permeability transition and resultant cytochrome *c* release.[34] Recently, a tumor-specific enhanced oxidative stress polymer conjugate (TSEOP) has been designed to boost tumor-specific antitumor immunity, by the release of cinnamaldehyde, which was proven to amplify ROS.[35]

In this paper, a series of cyclometalated Ir(III) complexes (**Ir1**−**Ir4**) with the structurally simple ligand (*E*)-2-styryl-1*H*-imidazo[4,5-*f*][1,10]phenanthroline (sip) was designed by the combination of a cinnamaldehyde group which can amplify ROS and an Ir(III) complex with good TP-PDT properties. The synthesis route and preparation procedure were optimized, so that the complexes could be obtained in apparently higher yield, productivity, and efficiency in comparison to the traditional methods. Their ground state and excited singlet and triplet state properties have been studied by spectroscopy, and density functional theory (DFT) and time-dependent DFT (TDDFT) calculations to discuss the effect of substituent groups on the photophysical properties of complexes. In-depth biological explorations of these Ir(III) complexes as highly sensitive TP mitochondria dyes and highly effective OP and TP excited PDT agents are presented. With both promising $^1O_2$ quantum yields and low dark toxicities, **Ir1**−**Ir4** showed remarkable phototherapeutic indexes (PIs) which are quite comparable to those of the most potent phototherapeutic Ir(III) complexes reported with structurally complicated ligands.

https://dx.doi.org/10.1021/acs.inorgchem.0c01509
Inorg. Chem. XXXX, XXX, XXX−XXX

EXPERIMENTAL SECTION

Instruments. ^{1}H NMR spectra were recorded on a Bruker Avance 300 or 400 spectrometer at 300 or 400 MHz. $^{13}C\{^1H\}$ NMR spectra were recorded on a Bruker Avance 600 spectrometer at 600 MHz. All chemical shifts are given relative to tetramethylsilane (TMS). Microanalysis (C, H, and N) was carried out with a PerkinElmer 240Q elemental analyzer. Electron spray ionization mass spectra (ESI-MS) were recorded on an AB QSTAR Pulsar mass spectrometer or an Agilent LC/MSD TOF mass spectrometer. IR spectra were recorded on an FT-IR Thermo Nicolet Avatar 360 spectrometer using a KBr pellet. UV−vis spectra were recorded on a Shimadzu UV-2700 spectrophotometer equipped with a temperature controller accessory and circulating water system. Emission spectra were recorded on an Agilent Cary Eclipse fluorescence spectrophotometer using $[Ru(bpy)_3]^{2+}$ (Φ_r = 0.028 in air-equilibrated water solution[36]) as the reference for calculating the quantum yield (Φ). The emission lifetimes of the Ir(III) complexes were recorded on an Edinburgh LFS-920 spectrometer with a hydrogen-filled excitation source. Cyclic voltammetry (CV) measurements were performed with a CH Instruments 840D electrochemical workstation. Samples were dissolved in acetonitrile (water ≤30 ppm by Karl Fischer) with 0.1 M tetrabutylammonium hexafluorophosphate ($TBAPF_6$) as a supporting electrolyte and the ferrocene/ferrocenium couple (Fc/Fc^+) used as an internal standard. A 3 mm diameter platinum-plate working electrode, a $Ag^+/AgCl$ (0.1 M $AgNO_3$ in acetonitrile) reference electrode, and a platinum-wire counter electrode were used. All potentials are reported relative to the ferrocene/ferrocenium couple (Fc/Fc^+). All experiments using one-photon excitation were performed with a blue light-emitting diode (LED) lamp (450 nm, 12 J cm^{-2}) as the light source. Two-photon photoluminescence spectra were recorded on a SpectroPro300i instrument, and the pump laser beam came from a Ti:sapphire laser system (pulse duration, 200 fs; repetition rate, 76 MHz; Coherent Mira900-D). TPA cross sections were measured by using the two-photon-induced fluorescence.[37]

Materials. The compounds 1,10-phenanthroline-5,6-dione[38] and $[Ir_2(ppy)_4(\mu\text{-}Cl)_2]$[39] (ppy = 2-phenylpyridine) were synthesized according to the literature methods. (*E*)-Cinnamaldehyde, (*E*)-4-nitrocinnamaldehyde, (*E*)-4-dimethylaminocinnamaldehyde, and ammonium hexafluorophosphate (NH_4PF_6) were purchased from Adamas-beta. (*E*)-4-Methoxycinnamaldehyde and silver triflate were purchased from Energy Chemical. Ammonium acetate, propanoic acid, aqueous ammonia, silica gel (200−300 mesh), *N*,*N*-dimethylformamide (DMF), acetonitrile (ACN), dichloromethane (DCM), ethanol (EtOH), and methanol (MeOH) were purchased from Greagent.

Synthesis and Characterization of Ir(III) Complexes. *[Ir(ppy)$_2$(sip)](PF$_6$) (**Ir1**).* A suspension of $[Ir_2(ppy)_4(\mu\text{-}Cl)_2]$ (1.340 g, 1.25 mmol), 1,10-phenanthroline-5,6-dione (phendione, 0.788 g, 3.75 mmol), and silver triflate (0.642 g, 2.5 mmol) in 100 mL of 1/1 (v/v) DCM/EtOH was stirred for 3 h under argon in a sealed reaction tube. The volume of the DCM/EtOH solution was reduced to 20 mL by reduced-pressure distillation and filtered. NH_4PF_6 (0.815 g, 5.0 mmol, in 2 mL of H_2O) was added, and $[Ir(ppy)_2(phendione)]PF_6$ (**Ir0**) precipitated as a yellow solid (2.01 g, 94% yield) upon standing at 0 °C. **Ir0** was dissolved in 100 mL of propanoic acid, and refluxed with (*E*)-cinnamaldehyde (0.330 g, 2.50 mmol) and ammonium acetate (3.88 g, 50.3 mmol) for 2 h. After it was cooled, the reaction mixture was poured into a 200 mL aqueous solution of NH_4PF_6 (2.00 g, 12.4 mmol) and neutralized with concentrated aqueous ammonia. The complex **Ir1** precipitated as an orange solid, which was isolated by suction filtration and washed with a small amount of cold methanol. The crude product was purified by flash column chromatography (4 cm in diameter and 6 cm in length) on silica gel (200−300 mesh) with DCM as eluent. Yield: 2.226 g, 92% based on $[Ir_2(ppy)_4(\mu\text{-}Cl)_2]$. Anal. Calcd for $C_{43}H_{30}F_6IrN_8P\cdot 2H_2O$: C, 51.44; H, 3.41; N, 8.37. Found: C, 51.21; H, 3.68; N, 8.09. ^{1}H NMR ($(CD_3)_2SO$, 300 MHz): δ 9.01 (d, J = 8.0 Hz, 2H), 8.87 (d, J = 8.5 Hz, 2H), 8.84 (d, J = 8.6 Hz, 2H), 8.23 (t, J = 7.8 Hz, 2H), 8.12 (d, J = 7.6 Hz, 2H), 8.07 (t, J = 4.7 Hz, 3H), 7.94 (d, J = 5.5 Hz, 1H), 7.91 (d, J = 5.4 Hz, 1H), 7.85 (d, J = 5.0 Hz, 3H), 7.79 (d, J = 6.7 Hz, 2H), 7.61 (q, J = 5.6 Hz, 4H), 7.49 (q, J = 6.4 Hz, 3H), 7.43 (t, J = 3.4 Hz, 1H), 7.35 (t, J = 6.5 Hz, 2H). $^{13}C\{^1H\}$ NMR ($CDCl_3$, 150 MHz): δ 168.2, 162.6, 148.4, 138.0, 136.9, 135.7, 131.9, 131.1, 129.1, 128.9, 127.6, 124.9, 123.3, 123.1, 122.8, 119.7, 115.5. FTIR (KBr) ν_{max} (cm^{-1}): 3334 (NH), 3086 (CH, aryl), 2962 (CH, aryl), 1606 (C═C, styryl), 1478 (C═C, aryl), 1387 (CN, pyridyl), 1110 (CN, imidazolyl), 848 (PF), 758 (C═C, aryl), 552 (PF). ESI-MS (MeOH, m/z): calcd for $C_{43}H_{30}IrN_8$ ($[M - PF_6]^+$), 823.22; found, 823.27.

*[Ir(ppy)$_2$(nsip)](PF$_6$) (**Ir2**).* This compound was synthesized according to the same procedure as for **Ir1**, using 0.442 g (2.50 mmol) of (*E*)-4-nitrocinnamaldehyde instead of (*E*)-cinnamaldehyde. Yield: 2.82 g, 93%. Anal. Calcd for $C_{43}H_{29}F_6IrN_7O_2P\cdot 2H_2O$: C, 49.24; H, 3.17; N, 9.35. Found: C, 48.98; H, 3.43; N, 9.07. ^{1}H NMR ($(CD_3)_2SO$, 300 MHz): δ 9.13 (d, 2H, J = 6.12 Hz), 8.28 (m, 4H), 8.16 (d, 2H, J = 3.21 Hz), 8,09 (m, 2H), 8.05 (m, 2H), 7.96 (d, 3H, J = 5.55 Hz), 7.89 (m, 3H), 7.68 (d, 1H, J = 12.36 Hz), 7.52 (d, 2H, J = 4.23 Hz), 7.07 (m, 2H), 6.98 (m, 4H), 6.30 (d, 2H, J = 5.58 Hz). $^{13}C\{^1H\}$ NMR ($(CD_3)_2SO$, 100 MHz): δ 167.4, 151.9, 150.8, 149.7, 149.0, 147.6, 144.8, 144.5, 142.6, 139.2, 133.0, 132.7, 131.7, 130.7, 128.7, 127.6, 125.5, 124.6, 124.3, 122.8, 121.7, 120.4. FTIR (KBr) ν_{max} (cm^{-1}): 3398 (NH), 3078 (CH, aryl), 2943 (CH, aryl), 1605 (C═C, styryl), 1523 (NO), 1415 (C═C, aryl), 1353 (CN, pyridyl), 1110 (CN, imidazolyl), 844 (PF), 749 (C═C, aryl), 566 (PF). ESI-MS (MeOH, m/z): calcd for $C_{43}H_{29}IrN_7O_2$ ($[M - PF_6]^+$), 868.20; found, 868.23.

*[Ir(ppy)$_2$(osip)](PF$_6$) (**Ir3**).* This compound was synthesized according to the same procedure as for **Ir1**, using 0.405 g (2.50 mmol) of (*E*)-4-methoxycinnamaldehyde instead of (*E*)-cinnamaldehyde. Yield: 2.22 g, 89%. Anal. Calcd for $C_{44}H_{32}F_6IrN_6OP\cdot 2H_2O$: C, 51.11; H, 3.51; N, 8.13. Found: C, 50.89; H, 3.76; N, 7.87. ^{1}H NMR ($(CD_3)_2SO$, 300 MHz): δ 12.13 (s, 1H), 9.31 (d, 1H, J = 5.91 Hz), 9.10 (d, 1H, J = 6.09 Hz), 8.17 (d, 1H, J = 3.45 Hz), 8.14 (d, 1H, J = 3.27 Hz), 7.94 (d, 2H, J = 6.12 Hz), 7.79 (m, 2H), 7.73 (m, 5H), 7.53 (d, 2H, J = 6.42 Hz), 7.42 (d, 1H, J = 3.9 Hz), 7.33 (d, 1H, J = 3.99 Hz), 7.12 (m, 3H), 6.99 (m, 2H), 6.92 (m, 1H), 6.81 (m, 3H), 6.42 (t, 2H, J = 6.39 Hz), 3.81 (s, 3H). $^{13}C\{^1H\}$ NMR (DMSO-d_6, 150 MHz): δ 168.1, 150.4, 148.8, 148.6, 148.0, 144.0, 138.0, 131.9, 130.9, 129.0, 128.8, 126.0, 124.8, 123.2, 122.7, 119.6, 112.0, 46.2. FTIR (KBr) ν_{max} (cm^{-1}): 3398 (NH), 3072 (CH, aryl), 2963 (CH, aryl), 1605 (C═C, styryl), 1462 (C═C, aryl), 1381 (CN, pyridyl), 1251 (CO), 1103 (CN, imidazolyl), 1028 (CO), 845 (PF), 763 (C═C, aryl), 593 (PF). ESI-MS (MeOH, m/z): calcd for $C_{44}H_{32}IrN_6O$ ($[M - PF_6]^+$), 853.23; found, 853.28.

*[Ir(ppy)$_2$(dsip)](PF$_6$) (**Ir4**).* This compound was synthesized according to the same procedure as **Ir1**, using 0.438 g (2.50 mmol) of (*E*)-4-dimethylaminocinnamaldehyde instead of (*E*)-cinnamaldehyde. Yield: 2.15 g, 85%. Anal. Calcd for $C_{45}H_{35}F_6IrN_7P\cdot 2H_2O$: C, 51.62; H, 3.75; N, 9.36. Found: C, 51.38; H, 3.93; N, 9.03. ^{1}H NMR ($(CD_3)_2SO$, 300 MHz): δ 9.19 (d, 2H, J = 6.03 Hz), 8.27 (d, 2H, J = 5.58 Hz), 8.12 (s, 2H), 8.04 (m, 2H), 7.96 (d, 2H, J = 5.49 Hz), 7.88 (m, 2H), 7.53 (m, 4H), 7.07 (m, 4H), 6.97 (m, 4H), 6.76 (d, 2H, J = 6.18 Hz), 6.58 (d, 1H, J = 3.81 Hz), 6.30 (d, 2H, J = 5.43 Hz), 2.98 (d, 6H, J = 12.36 Hz). $^{13}C\{^1H\}$ NMR (DMSO-d_6, 150 MHz): δ 168.1, 160.4, 154.1, 148.7, 148.2, 143.7, 138.0, 136.4, 131.9, 130.9, 129.0, 128.6, 124.8, 122.8, 123.3, 123.1, 119.6, 114.1, 113.3, 55.3. FTIR (KBr) ν_{max} (cm^{-1}): 3397 (NH), 3058 (CH, aryl), 2904 (CH, aryl), 1605 (C═C, styryl), 1531 (C═C, aryl), 1476 (CN, pyridyl), 1361 (CN, $-NMe_2$), 1123 (CN, imidazolyl), 838 (PF), 763 (C═C, aryl), 546 (PF). ESI-MS (MeOH, m/z): calcd for $C_{45}H_{35}IrN_7$ ($[M - PF_6]^+$), 866.32; found, 866.26.

Singlet Oxygen Quantum Yields. Φ_Δ for $^1O_2$ generation in air-saturated MeOH was determined by monitoring the photo-oxidation of 1,3-diphenylisobenzofuran (DPBF) promoted by the Ir(III) complex. The absorbance of DPBF was adjusted to 1.0 at 409 nm in air-saturated MeOH, and the absorbance of the Ir(III) complex was adjusted to 0.1 at the irradiation wavelength. The photo-oxidation of DPBF was monitored at the interval of 10 s. The Φ_Δ value for $^1O_2$ was calculated by a relative method using RB ($\Phi_{\Delta std}$ = 0.76 in air-saturated MeOH) as the reference.[40] Similarly, the $^1O_2$ generation

https://dx.doi.org/10.1021/acs.inorgchem.0c01509
Inorg. Chem. XXXX, XXX, XXX−XXX

Scheme 1. Synthetic Route of Cyclometalated Ir(III) Complexes in This Study

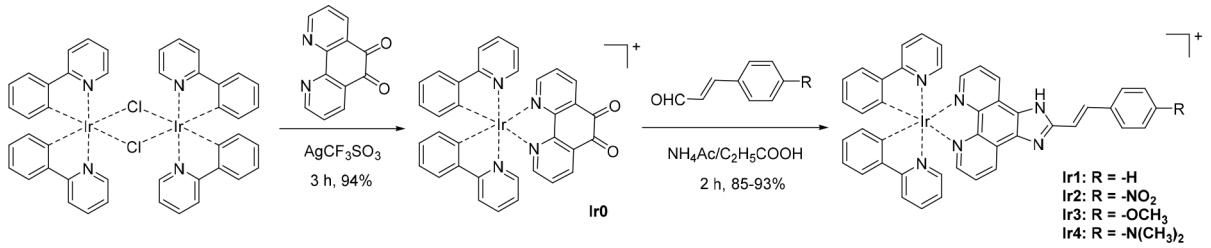

quantum yields in air-saturated aqueous solution Φ_{Δ}(aq) were also determined, using *N*,*N*′-bis(2,3-dihydroxypropyl)-9,10-anthracenedipropanamide (DHPA) instead of DPBF.

Quantum Chemistry Calculations. The DFT calculations were carried out with the Gaussian 09 program package[41] using the M06 (hybrid meta exchange-correlation functionals, which were parametrized including both transition metals and nonmetals and containing dispersion correction) method and LanL2DZ basis set (a double-ζ basis set containing effective core potential).[42] Full geometry optimization computations were carried out. The stability of the optimized conformation of the complexes was confirmed by a frequency analysis, which showed no imaginary frequency for each energy minimum. Both geometry optimization and optical property calculations were performed in water using the conductor polarized continuum model (CPCM).[43] For absorption spectral calculations, the 80 lowest singlet excited states were calculated to reproduce the experimental spectra in the 250−600 nm range. The discrete optical transitions with their corresponding oscillator strengths were broadened by a Gaussian function with a full width at half-maximum (fwhm) of 3000 cm^{-1} to represent an experimental inhomogeneous spectral broadening. To obtain the triplet (phosphorescence) and singlet (fluorescence) emission energies, the molecular structures of the lowest singlet excited state (S1) and lowest triplet excited state (T1) were optimized using analytical TDDFT gradients. A compact representation of an excited state via a photoexcited electron−hole pair, which fits for chemical intuition, can be obtained using natural transition orbitals (NTOs).[44] When NTO calculations were performed, an electron−hole pair transition from a ground state to an excited state could be realized through unitary transformation of the transition density matrix of a specific excited state.[44] NTO pairs contributing to the most important optical transitions were visualized for plotting excited charge densities by setting the isovalue as 0.02. For phosphorescence, we also used an additional method based on the ΔSCF approach,[45] which is computationally less expensive than the optimization of the excited state and provides relatively accurate results because of the inclusions of orbital relaxations. It involves a geometry optimization on the ground triplet state using unrestricted DFT and then a TDDFT calculation of a few lowest triplet excited states using that ground-state triplet geometry.[46]

DNA Binding Experiments. Calf thymus DNA (CT-DNA) was obtained from the Sigma Co. The preparation of the DNA stock solution, determination of the DNA concentration, and DNA-binding experiments of the Ir(III) compounds, including absorption spectral titration, viscosity measurements, and thermal denaturation studies, were performed as described previously.[47]

Two-Photon Confocal Laser Scanning Microscopy. The stock solutions (100 μM) of Ir(III) complexes for cell experiments were prepared in PBS containing 1% (v/v) DMSO (Sangon). Human lung cancer cell lines A549 were grown on a 6 Chamber Glass Slide (Thermo Fisher Scientific, USA) at a density of 6×10^4 cells/mL and incubated for 1 h with the Ir(III) compounds at 10 μM in PBS containing 0.1% (v/v) DMSO. The cells were washed twice with PBS for 5 min. Nuclei and mitochondria were counterstained with 1.0 μg/mL of DAPI (4′,6-diamidino-2-phenylindole, Solarbio) and 0.2 μM MTG (MitoTracker Green, Invitrogen) for 30 min and washed with PBS twice for 5 min. The two-photon laser microscopy system consisted of a Nikon A1plus confocal microscope (Apo LWD 25*x*/1.10 DIC N2 Objective, Galvano Scanner, NDD Reflect Detector, IR-DM First Dichroic Mirror) and a COHERENT Chameleon Vision II widely tunable laser (800.0 nm, 140 fs, 3.5 W, 80 MHz). Fluorescence images were collected on three detection channels (blue, 420 nm; green, 515 nm; red, 590 nm) and processed by NIS Elements (Nikon) software. Z-stack images (12 loops) were collected with 800.0 nm excitation wavelength and 575.0 nm emission wavelength. The Pearson correlation coefficients (*R*) were calculated by ImageJ (1.53a) software[48] for the colocalization of MTG and Ir(III) complexes.

Photocytotoxicity. The photocytotoxicity of **Ir1**−**Ir4** toward three human cancer cell lines (lung A549, breast MCF7, and prostate 22Rv1) were tested by both one- and two-photon excitation techniques. Exponentially grown cancer cells were seeded in triplicate into 384-well plates at 1×10^4 cells per well. After incubation for 24 h, the cells were treated with increasing concentrations of the tested complexes. The culture medium alone was used as the blank. The plates were incubated in the dark for 24 h. Then, all of the culture media were refreshed. For the cell cultures exposed to light, all wells were irradiated by a one- or two-photon light source for 10 min and incubated for an additional 48 h. Finally, IC_{50} values of the compounds in the two groups were measured by plotting the percentage of viability that was tested by a CCK-8 kit (Sigma) versus concentration on a logarithmic graph. The cell survival rate in the control wells of the dark group was considered to represent 100% cell survival. Phototherapeutic indexes (PIs) were calculated from the ratio of dark to light IC_{50} values.

RESULTS AND DISCUSSION

Synthesis. Most current synthesis routes of $[Ir(ppy)_2L]^+$ type compounds have involved the reaction between $[Ir_2(ppy)_4(\mu\text{-}Cl)_2]$ and L, which usually required at least a 3-fold excess of L to complete the conversion of $[Ir_2(ppy)_4(\mu\text{-}Cl)_2]$. As more and more complicated structures of L were designed for diverse functions of interest and synthesized with more and more steps, this synthetic route has become less and less efficient. Here we present an optimized route for the preparation of $[Ir(ppy)_2L]^+$ type complexes (Scheme 1). $[Ir(ppy)_2(phendione)]PF_6$ (**Ir0**) was first prepared with the relatively economical 1,10-phenthroline-5,6-dione as L. The obtained **Ir0** was sufficiently pure to proceed to the next reaction without column chromatography. **Ir1**−**Ir4** were then synthesized by the condensation of **Ir0** and cinnamaldehydes. The overall yields based on $[Ir_2(ppy)_4(\mu\text{-}Cl)_2]$ and aldehydes were 85−93%, which greatly improved the economy of both the precious metal iridium and the material for ligand synthesis. Although the cinnamaldehydes used in this paper are inexpensive, this is a very economical synthetic route for other precious aldehyde materials. These four Ir(III) complexes could be prepared by a simple two-step reaction with apparently higher yield, productivity, and efficiency in comparison to the traditional reactions, facilitating its further application in animal experiments and pharmaceutical preparations. The prepared Ir(III) complexes have been characterized by ^1H NMR, ^{13}C NMR, IR, ESI-MS, and

https://dx.doi.org/10.1021/acs.inorgchem.0c01509
Inorg. Chem. XXXX, XXX, XXX−XXX

elemental analysis. **Ir1**−**Ir4** have good solubility in water. With 5% (v/v) DMSO, the concentration of the stock solution could reach 400 μM in water or phosphate-buffered saline (PBS).

Electronic Absorption. The UV−vis absorption spectra of complexes **Ir1**−**Ir4** were recorded in MeOH at room temperature (Figure 2), and the absorption band maxima

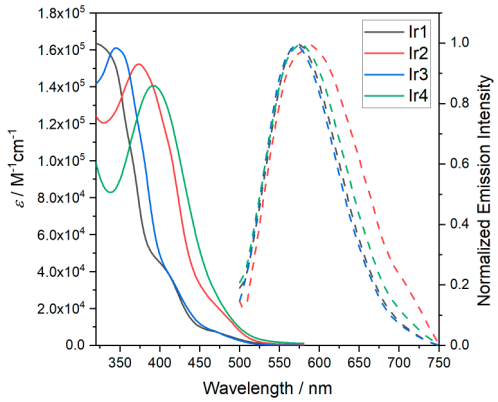

Figure 2. Absorption (solid) and normalized emission spectra (dashed) of **Ir1**−**Ir4** in air-saturated MeOH solution. The excitation wavelengths are 404, 418, 416, and 392 nm for **Ir1**−**Ir4**, respectively.

and molar extinction coefficients (ε) are summarized in Table 1. The absorption follows the Beer−Lambert law in the concentration range of 1−100 μM, suggesting the absence of ground state aggregation in this tested concentration range. The absorption spectra for Ir(III) complexes are comprised of two main absorption bands (an intense band below 400 nm and a weaker band extended to 404−473 nm), in line with the reported Ir(III) complexes with extended π-conjugated diamine (N^N) ligands.[46,49,50]

To better understand the effect on the absorption spectra of the substituent groups on the N^N ligand, DFT calculations were performed for **Ir1**−**Ir4**. As we have focused on the biological applications of the Ir(III) complexes in this paper, the solvent effect was implicitly included by CPCM for water in the theoretical study and discussed with the experimental data in aqueous solution as well. The optimized structures showed that all complexes adopted a similar octahedral geometry around the Ir(III) center and the dihedral angles within the N^N ligand are very close to 0 or 180° (Figure S1). The calculated electron density distributions of the HOMO and LUMO are different for the four complexes (see the representative frontier molecular orbital plots for **Ir1**−**Ir4** in Figure S1). For **Ir1**−**Ir3**, the HOMOs are delocalized on the ppy ligand and the d orbital of the Ir(III) ion and the LUMOs are exclusively on the ligand, similar to the case for $[Ir(ppy)_2(bpy)]^+$ (bpy = 2,2′-bipyridine) and some other $[Ir(ppy)_2L]^+$ type complexes.[40] For **Ir4**, however, the HOMO is delocalized on the styryl part of the N^N ligand (location of HOMO-1 energy levels for **Ir1**−**Ir3**). The MO which is delocalized on the ppy ligand and the d orbital of the Ir(III) ion (HOMOs for **Ir1**−**Ir3**) for **Ir4** lowers to HOMO-1. This difference on the MO population is thought to be the result of a conjugation function between the lone pair on the N atom and phenyl ring for **Ir4**, as the optimized structure showed the two $-CH_3$ groups are located nearly coplanar with the phenyl group of sip.

These different frontier MO populations give rise to different ground state energy levels and excitation properties. The ground state energy diagram for **Ir1**−**Ir4** is shown in Figure 3, and the calculated electronic absorption spectral data

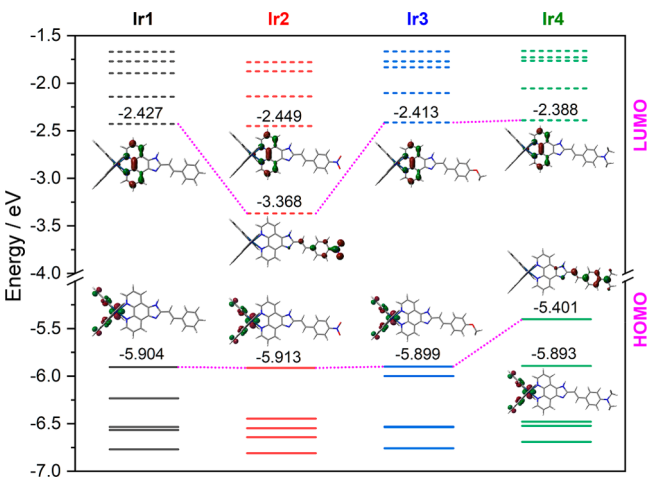

Figure 3. Ground state energy diagram for **Ir1**−**Ir4** (M06/Lanl2dz). The solvent water was included by the conductor polarized continuum model (CPCM).

(wavelengths, oscillator strengths, excitation energies, assignments of contributions to excited states) and their comparisons with the corresponding experimental data in aqueous solution are summarized in Table S1. The simulated absorption spectra are in good accordance with the experimental spectra (Figure S2). For **Ir1**−**Ir3**, there are two theoretical metal to ligand charge transfer (MLCT) transitions. The first MLCTs (HOMO → LUMO) are mixed with ligand to ligand charge transfer (LLCT) transitions ($\pi_{ppy} \rightarrow \pi^*_{sip}$), and the calculated

Table 1. Photophysical[a] and Electrochemistry[b] Data for Ir(III) Complexes

complex	absorption/nm[c] (ε/10^3 M^{-1} cm^{-1})	emission/nm (Φ)	Φ_Δ	Φ_Δ(aq)[d]	τ/ns	δ^e/GM	E_{ox}/V	E_{red}/V	E_{gap}/V	ΔE/eV
Ir1	468 (sh, 3.8), 404 (sh, 2.2), 365 (51.2), 342 (sh, 77.0)	572 (0.12)	0.85	0.24	875	162	+0.80	−1.28, −1.62, −2.14	2.08	3.48
Ir2	473 (sh, 10.2), 418 (sh, 46.7), 373 (76.2)	590 (0.04)	0.37	0.14	836	113	+0.84	−1.12, −1.52, −2.08	1.96	2.54
Ir3	467 (sh, 4.1), 416 (sh, 18.5), 357 (sh, 77.6), 344 (80.5)	572 (0.18)	0.95	0.31	942	168	+0.78	−1.36, −1.54, −2.04	2.14	3.49
Ir4	473 (sh, 13.0), 392 (70.3)	577 (0.03)	0.57	0.17	851	152	+0.76, +0.50	−1.42, −1.58, −2.12	1.92	3.01

[a]In air-saturated MeOH solution (2×10^{-5} M), except for Φ_Δ(aq). [b]Cyclic voltammograms performed at a scan rate of 200 mV s^{-1} versus Fc/Fc$^+$ using 0.1 M $TBAPF_6$ as a supporting electrolyte in degassed MeCN. [c]Shoulder peaks are marked as sh. [d]In aqueous solution (2×10^{-5} M). [e]Two-photon absorption cross sections (δ) upon excitation at λ_{ex} = 800 nm (1 GM = 10^{-50} cm^4 s photon^{-1}).

https://dx.doi.org/10.1021/acs.inorgchem.0c01509
Inorg. Chem. XXXX, XXX, XXX−XXX

Table 2. Natural Transition Orbitals (NTOs) for Low-Energy Transitions of Ir1−Ir4

Compound (λ_{Em} / nm)[a]	Excited State	Hole	Electron	Excited State[b]	Hole	Electron
Ir1 (600)	S1 591 nm (f = 0.0008)	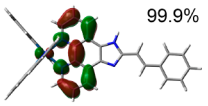 99.9%	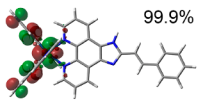 99.9%	T1 611 nm (608 nm)	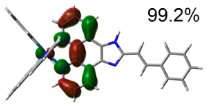 99.2%	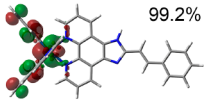 99.2%
	S2 456 nm (f = 0.4089)	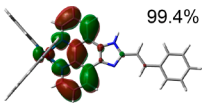 99.4%	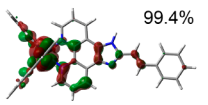 99.4%	T2 577 nm	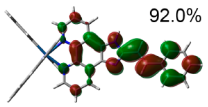 92.0%	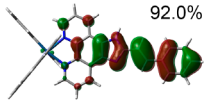 92.0%
Ir2 (685, 641)	S1 710 nm (f = 0.0000)	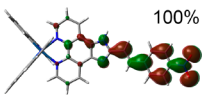 100%	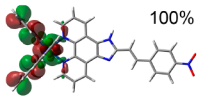 100%	T1 1131 nm (904 nm)	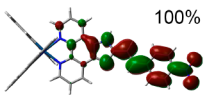 100%	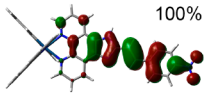 100%
	S2 550 nm (f = 1.2657)	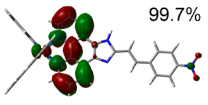 99.7%	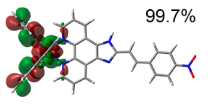 99.7%	T2 640 nm	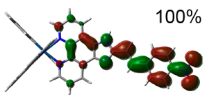 100%	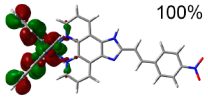 100%
Ir3 (718, 603)	S1 589 nm (f = 0.0008)	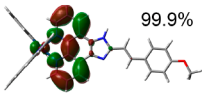 99.9%	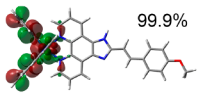 99.9%	T1 963 nm (769 nm)	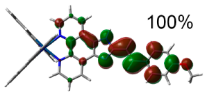 100%	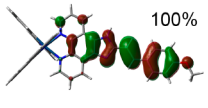 100%
	S2 472 nm (f = 0.4345)	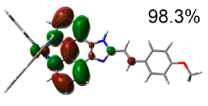 98.3%	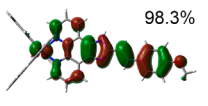 98.3%	T2 535 nm	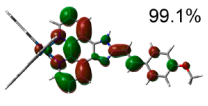 99.1%	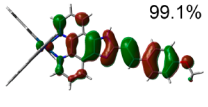 99.1%
Ir4 (697, 632)	S1 598 nm (f = 0.3177)	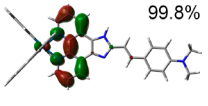 99.8%	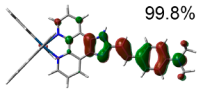 99.8%	T1 712 nm (699 nm)	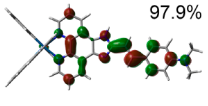 97.9%	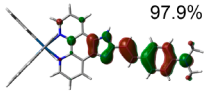 97.9%
	S2 543 nm (f = 0.0009)	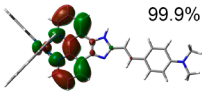 99.9%	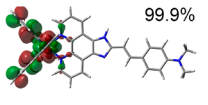 99.9%	T2 629 nm	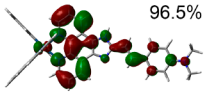 96.5%	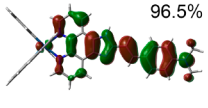 96.5%

[a]Experimental emission wavelengths in aqueous solution. [b]Triplet emission wavelengths calculated by TDDFT optimized excited triplet state geometries. Values in parentheses represent the emission wavelengths calculated by the ΔSCF approach.

oscillator strengths (f) are very low (from 0 to 0.0004). Therefore, the second MLCTs H-2 → LUMO (f = 0.1244) for Ir1, H-1 → LUMO (f = 1.0447) for **Ir2**, and H-3 → LUMO (f = 0.1782) for **Ir3** are considered as major contributions to the MLCT absorptions (the weaker absorption bands above 400 nm) of their complexes. The stronger absorption bands between 400 and 360 nm are attributed to the intraligand (IL) transitions of sip-type ligands ($\pi_{sip} \rightarrow \pi^*_{sip}$). Due to the different MO population of **Ir4**, some strong IL transitions appear at longer wavelength, giving its MLCT band partial intraligand character. As a result, **Ir4** has a longer absorption wavelength in comparison to the other three complexes.

Natural transition orbital (NTO) calculations were also performed to explore the characters of the above optical transitions. Cartesian coordinates of the optimized structures of **Ir1**−**Ir4** for the ground state (S0, DFT), first excited singlet state (S1, TDDFT), and first excited triplet state (T1, TDDFT) are given in Tables S2−S5. As indicated by the NTOs (Table 2), the holes in all complexes were primarily localized on the N^N ligands and the d orbital of the Ir(III) ion. The electron-density distribution calculations show that the HOMO → LUMO transition played the major role (99.4−100%) in generating the S1 excited state and the substituent groups had an apparent effect on the hole energy. Therefore, it is important to analyze how structural modifications influenced the HOMO and LUMO energy levels. As displayed in the ground-state energy diagram (Figure 3), an electron-withdrawing group (−NO_2 in **Ir2**) lowered the energy level of both the HOMO and LUMO, while an electron-donating group (−OMe in **Ir3** and −NMe_2 group in **Ir4**) raised the energy level of the HOMO and LUMO. The HOMO−LUMO energy gaps in **Ir2** and **Ir4** are apparently smaller than those in **Ir1** and **Ir3**. In view of the direct relationship between the frontier molecular orbital energy level and the redox potential, the

https://dx.doi.org/10.1021/acs.inorgchem.0c01509
Inorg. Chem. XXXX, XXX, XXX−XXX

electrochemical properties of complexes **Ir1**−**Ir4** were then investigated.

Electrochemistry. To confirm the effect of substituent groups on the HOMO−LUMO gaps in **Ir1**−**Ir4**, ground state redox potentials of **Ir1**−**Ir4** were investigated in degassed anhydrous CH_3CN solutions by CV using the Fc^+/Fc couple as the internal standard. **Ir1**−**Ir3** showed an irreversible couple from 0.78 to 0.84 V (Table 1 and Figure S3), which was assigned to Ir(IV)/Ir(III) oxidation.[40,51,52] For **Ir4**, however, two oxidation couples were observed. This experimental result could be explained by the DFT calculations. As illustrated in Figure 3, the HOMO of **Ir4** is composed of the π orbital of N^N ligand and its energy level is obviously higher than those of **Ir1**−**Ir3**. The occupied d orbital of Ir(III) in **Ir4** mainly populates on HOMO-1, with an energy level close to that of the HOMO of **Ir1**−**Ir3** and a similar orbital population. Therefore, the two oxidation couples at 0.50 and 0.76 V were attributed to be the oxidation of the N^N ligand and Ir(III) ion, respectively.

Three reduction couples (from −1.12 to −1.42 V, from −1.52 to −1.62 V, and from −2.04 to −2.14 V) were observed for **Ir1**−**Ir4**, representing the reduction of sip and two ppy ligands, comparable to the case for similar Ir(III) complexes.[51−53] The trend of the electrochemical energy gaps (E_{gap}) of these complexes matches well with the trend of the calculated HOMO−LUMO gaps (ΔE), although there appears to be some discrepancy in the absolute values of ΔE with E_{gap}. Therefore, the DFT calculations clearly explained the trend in energy level shifts upon modification by different substituent groups. A similar discrepancy between the calculated HOMO−LUMO gaps and the electrochemical energy gaps has been reported in other Ir(III) complexes.[54,55]

Photoluminescence. Photoluminescent properties are of great importance to Ir(III) complexes in many application fields, such as organic light-emitting diodes (OLEDs), solar energy conversion, luminescent biological labeling, etc.[56] Because the emission of Ir(III) complexes typically originates from the excited triplet state, the emission characteristics of **Ir1**−**Ir4** at room temperature were investigated to understand the effects of substitution on the excited triplet states with the assistance of DFT calculations.

The emission spectra of **Ir1**−**Ir4** in water are displayed in Figure S4, and the emission band maxima are summarized in Table 2, together with theoretical data obtained by excited triplet state DFT calculations and NTO analysis. In order to intuitively reflect the photoluminescent properties and relative intensity of each compound, all compounds used the exact same measurement conditions, such as compound concentration, excitation wavelength, slit width, detector voltage, etc., and the resulting emission spectra were not normalized. The emission spectrum of **Ir1** (single peak at 600 nm) was structureless, which is a characteristic of ^{3}CT state (^{3}MLCT/^{3}LLCT) emission.[57−59] The theoretical emission wavelength obtained by TDDFT calculations (611 nm) was in good accordance with the experimental data. The spin-density distributions shown in Table 2 for **Ir1** agree well with the NTOs representing the excitation from S0 to T1 (99.2% for ^{3}MLCT/^{3}LLCT states). In contrast, the emission spectra of **Ir2**−**Ir4** were apparently red shifted in comparison to **Ir1** and exhibited clear vibronic structures (shoulder peaks at 685, 718, and 697 nm for **Ir2**−**Ir4**, respectively), suggesting that the emission of these three complexes emanated from the intraligand (IL, ligand-centered $^3\pi,\pi^*$ state) transition.[53] NTOs obtained by the TDDFT calculations also supported this attribution (Table 2). The spin density of S0 to T1 excitation for **Ir2**−**Ir4** was mainly distributed on the sip-type ligands for both holes and electrons, and the theoretical contributions for these ^{3}IL transitions were 97.9−100%. These ^{3}IL transitions have been proven to be very important for a metal-based PDT agent to sensitize $^1O_2$, such as TLD1433.[32]

The advantage of TDDFT calculations is that they can provide specific information about the excited-state transitions shown above. However, the calculation results of the excitation energy deviated greatly from the experimental data. Therefore, an additional calculation based on the ΔSCF approach[45] was performed, which provides more accurate results because of the inclusion of orbital relaxations. As shown in Table 2, the S0 to T1 excitation energies obtained by the ΔSCF approach were much closer to the experimental data, providing support for the rationality of theoretical calculation results. The above studies of fluorescence properties and calculations of excited states have revealed the luminescent nature of this class of compounds and how the substituents affected their luminescent properties, which could have important implications for the design of Ir(III)-based cellular photoluminescent dyes and photosensitizers for PDT.

Singlet Oxygen Quantum Yield. To estimate the efficiency of $^1O_2$ generation, which is essential for PDT, the $^1O_2$ generation quantum yields (Φ_Δ) for all Ir(III) complexes were measured by monitoring the time-dependent absorbance of DPBF at 409 nm (Table 1 and Figure S5). The Φ_Δ values for **Ir1** and **Ir3** were found to be 0.85 and 0.95, indicating a high $^1O_2$ generation efficiency. **Ir3** has a higher Φ_Δ value than **Ir1**. On one hand, this may be due to the electron-withdrawing effect of the methoxy group. It have also been observed recently that Φ_Δ values of similar Ir(III) complexes increased greatly by the introduction of electron-donating substituents.[40] On the other hand, the higher triplet quantum yield (stronger emission intensity) of **Ir3**, as discussed above in the photoluminescence section (Figure S4), might also contribute to its higher Φ_Δ value, because the efficiency of $^1O_2$ generation was considered to be relative to the triplet excited state energy and quantum yield.[40] Therefore, it would not be surprising that **Ir2** has a very low $^1O_2$ generation efficiency (Φ_Δ = 0.37), because its low emission intensity (Figure S4) and strongly electron withdrawing substituent ($-NO_2$). Although **Ir4** has an electron-donating substituent ($-NMe_2$), its triplet excited state energy level and quantum yield are much lower than those of **Ir1** and **Ir3**. The $^1O_2$ generation efficiency of **Ir4** (Φ_Δ = 0.57) suggested that the triplet quantum yield played a more important role than the electronic effect of the substituent group. These studies suggested that the $^1O_2$ generation efficiency is tunable via simple substitution on the sip ligand, and the higher Φ_Δ values might result in a better performance of **Ir1** and **Ir3** in cell imaging and PDT. Similarly, the $^1O_2$ generation quantum yields in aqueous solution Φ_Δ(aq) were also determined (Table 1), using DHPA instead of DPBF. All the tested Φ_Δ(aq) values are higher than those of the reported cyclometalated Ir(III) complexes.[60]

Two-Photon-Absorption (TPA) Cross Sections. To examine the TPA properties of **Ir1**−**Ir4**, the TPA cross sections (δ) of these compounds were also investigated, using RB as the standard. The TPA cross sections of the complexes were 113−168 GM (1 GM = 10^{-50} cm^4 s photon^{-1}), as shown in Table 1. As suggested by Furuta, δ values should be higher than 0.1 GM for optical imaging applications in live

https://dx.doi.org/10.1021/acs.inorgchem.0c01509
Inorg. Chem. XXXX, XXX, XXX−XXX

specimens.[61] The δ values of **Ir1**−**Ir4** not only meet the requirements mentioned above but are also 2-fold higher than those of similar mononuclear Ir(III) complexes.[60] However, the δ values of **Ir1**−**Ir4** are lower than those of some dinuclear Ir(III) complexes.[37]

Cellular Localization by Two-Photon Confocal Laser Scanning Microscopy. After confirming that **Ir1**−**Ir4** can efficiently produce $^1O_2$ upon light irradiation, we investigated their cellular uptake and cellular localization. The cellular localization of **Ir1**−**Ir4** was investigated by confocal laser scanning microscopy (CLSM) on human lung cancer cells A549 in PBS containing 0.1% (v/v) DMSO. As shown in Figure 4, all Ir(III) complexes showed strong red luminescence

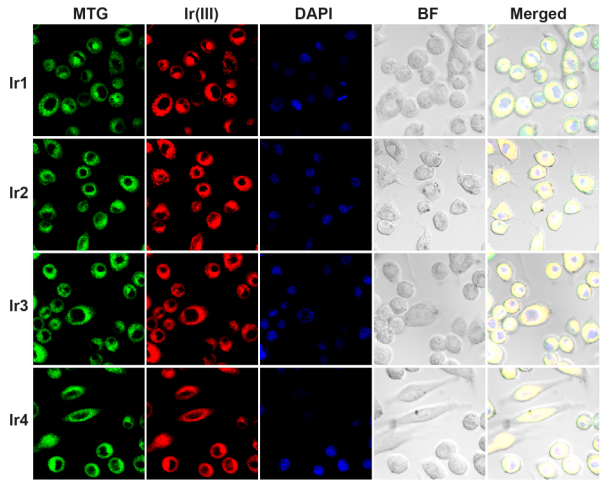

Figure 4. Cellular localization of **Ir1**−**Ir4** by two-photon confocal laser scanning microscopy on human cancer cells A549 in PBS containing 0.1% (v/v) DMSO: MTG, mitochondrion dye, green channel; Ir(III), **Ir1**−**Ir4**, red channel; DAPI, nucleus (DNA) dye, blue channel; BF, bright field; Merged, overlay of the four channels on the left.

within the cells under TP excitation (800 nm). The specific cellular target of **Ir1**−**Ir4** was further confirmed by colocalization assays. The signals of **Ir1**−**Ir4** overlapped well with the that of commercial mitochondrion-specific dye MTG. In contrast, a poor correlation coefficient was found when the nucleus dye DAPI was used. Therefore, mitochondria are the main target of **Ir1**−**Ir4** in A549 cells. In order to confirm this conclusion, Pearson correlation coefficients (R) have been calculated for the colocalization between MTG and Ir(III) complexes (Figure S6). The values of R reached 0.91−0.94 for **Ir1**−**Ir4**, suggesting a very high colocalization. The fact that **Ir1**−**Ir4** target on mitochondria may be beneficial for their PDT activity, because a mitochondria-targeted Ir(III) complex has been found to exhibit an improved PDT effect in comparison to a lysosome-targeted Ir(III) complex with similar photophysical properties and $^1O_2$ quantum yields, especially under hypoxia conditions.[62]

Moreover, as displayed in the Z-stack images (Figure S7), all Ir(III) complexes gave clear fluorescence photos of the entire cells at 12 increasing depths. It can be assumed, not arbitrarily, that a 3D image of the mitochondria in the whole cell can be obtained by setting a small enough scanning interval.[63] Therefore, these Ir(III) complexes have good potential as highly sensitive cellular mitochondrial dyes and PDT agents.

In Vitro Photodynamic Therapy Studies by One- and Two-Photon Technology. The toxicities of **Ir1**−**Ir4** on three human tumor cell lines (A549, MCF7 and 22Rv1) were first investigated in the dark to assess whether the compounds were nontoxic, which is an important property for a PDT agent. It is encouraging that all compounds were found to be nontoxic toward these cells in the absence of light (IC_{50} > 160 μM, Table 3). The phototoxicities of the Ir(III) complexes on the same tumor cell lines were then investigated. For OP-PDT (450 nm, irradiated for 10 min and incubated for 48 h), all Ir(III) compounds became highly toxic. Cells untreated by Ir(III) complexes were also exposed to the same irradiation procedure and found not to be affected. Among the three different tumor cell lines studied, all Ir(III) complexes showed a better inhibitory effect on A549 cells (Table 3), in comparison to MCF7 and 22Rv1 cells. **Ir3** has the highest inhibitory activity for the three tested cell lines among the four Ir(III) complexes. The photocytotoxicity of **Ir3** to A549 cells tested by the one-photon excitation (OPE) technology reached an IC_{50} value as low as 1.35 μM (PI-1 = 179). Under similar experimental conditions, the clinically approved PDT agent 5-aminolevulinic acid (5-ALA) displayed a lower phototoxicity and a lower PI in comparison to the Ir(III) complexes studied in this work. $[Ir(tpy)(pbpz)Cl]^+$ has the highest activity and PI among the four Ir(III) complexes.[64] Although the OPE IC_{50} value of $[Ir(tpy)(pbpz)Cl]^+$ is lower than that of **Ir3** in this study, its dark cytotoxicity is much higher. Therefore, PI-1 for **Ir3** is over 2-fold that of $[Ir(tpy)(pbpz)Cl]^+$.

The TP-PDT experiments were then performed under the same cell conditions, except for the 800 nm laser light source. All Ir(III) complexes showed higher phototoxicity toward the three tested tumor cell lines (Table 3). The two-photon excitation (TPE) phototoxicity index values (PI-2) for all Ir(III) complexes were also apparently larger in comparison to those irradiated by 450 nm light (Table 3). Cisplatin, as a traditional chemotherapeutic drug without PDT activity, showed no significant difference in toxicity (PI = 1.00−1.15), under dark, OPE, or TPE conditions. As the most promising compound of the series, **Ir3** showed a very high photocytotoxicity to A549 cells (IC_{50} value as low as 0.96 μM, PI-2 = 253), as tested by TPE technology. This exciting experimental result was obtained by simply improving an experimental operation—the use of 384-well plates. Usually, 96-well plates are used for in vitro PDT experiments. However, the TP laser is concentrated, and it is difficult to cover the entire well area. Therefore, the cell viability estimation is more difficult, and a precise cell viability test has to be performed only in the irradiated area.[22] This limitation can nevertheless be overcome by using 384-well plates and a low-magnification objective, which allow scanning the whole well with the laser.[65] By plating the same number of cells in the 96-well plate into the 384-well plate, the number of cells per volume increased significantly, which allowed the experimental results to show the effect of light penetration on cell viability. In this study, the superiority in phototoxic properties of **Ir1**−**Ir4** irradiated by 800 nm light to those irradiated by 450 nm light should be attributed to the excellent penetration of infrared light. The IC_{50} values toward three different tumor cell lines correlate well with their efficiency in $^1O_2$ generation (**Ir3** > **Ir1** > **Ir4** > **Ir2**). Surprisingly, the dark toxicity of **Ir2** is very low (418−704 μM), giving it a higher than expected PI value. This could be considered as an advantage for the PDT properties of **Ir2**.

https://dx.doi.org/10.1021/acs.inorgchem.0c01509
Inorg. Chem. XXXX, XXX, XXX−XXX

Table 3. (Photo)cytotoxicity (IC_{50}, μM) of Ir1−Ir4 toward Three Human Tumor Cell Lines

compound	A549			MCF7			22Rv1		
	dark[a]	OPE[b] (PI-1)[d]	TPE[c] (PI-2)[e]	dark[a]	OPE[b] (PI-1)[d]	TPE[c] (PI-2)[e]	dark[a]	OPE[b] (PI-1)[d]	TPE[c] (PI-2)[e]
Ir1	362 ± 28.2	5.37 ± 0.36 (67.4)	3.73 ± 0.26 (97.0)	224 ± 20.6	7.86 ± 0.56 (28.5)	5.53 ± 0.42 (40.5)	205 ± 17.8	8.52 ± 0.68 (24.1)	6.49 ± 0.43 (31.6)
Ir2	704 ± 51.6	8.76 ± 0.69 (80.4)	6.38 ± 0.72 (110)	463 ± 51.7	9.72 ± 0.72 (47.6)	8.43 ± 0.85 (49.1)	418 ± 34.6	13.6 ± 0.83 (30.7)	11.7 ± 0.96 (35.7)
Ir3	242 ± 18.2	1.35 ± 0.14 (179)	0.96 ± 0.08 (253)	164 ± 10.3	4.31 ± 0.27 (38.1)	2.84 ± 0.14 (57.7)	187 ± 13.6	6.36 ± 0.52 (29.4)	4.51 ± 0.23 (41.5)
Ir4	314 ± 26.4	5.91 ± 0.06 (53.1)	3.86 ± 0.42 (81.3)	216 ± 18.5	9.24 ± 0.37 (23.4)	7.61 ± 0.81 (28.4)	263 ± 19.0	9.72 ± 0.76 (27.1)	7.13 ± 0.52 (36.9)
cisplatin	1.24 ± 0.10	1.08 ± 0.08 (1.15)	1.13 ± 0.09 (1.10)	1.05 ± 0.06	1.01 ± 0.06 (1.04)	1.04 ± 0.05 (1.00)	1.13 ± 0.07	1.04 ± 0.06 (1.09)	1.09 ± 0.06 (1.04)
5-ALA[f]	175 ± 8.40	34.1 ± 2.30 (5.13)	116 ± 5.42 (1.51)	182 ± 9.43	38.7 ± 3.13 (4.70)	124 ± 6.81 (1.47)	162 ± 7.28	32.7 ± 2.94 (4.95)	97.5 ± 7.48 (1.66)
$[Ir(tpy)(pbpz)Cl]^+$[g]	56.6 ± 0.2	0.6 ± 0.1 (94.3)							

[a]The IC_{50} values in the dark (incubated for 24 h). [b]The IC_{50} values under one-photon excitation (450 nm, irradiated for 10 min and incubated for 48 h). [c]The IC_{50} values under two-photon excitation (800 nm, irradiated for 10 min and incubated for 48 h). [d]PI-1 is the phototoxicity index for one-photon excitation, which is the ratio between the IC_{50} values in the dark and those under one-photon excitation. [e]PI-2 is the phototoxicity index for two-photon excitation, which is the ratio between the IC_{50} values in the dark and those under two-photon excitation. [f]Measured IC_{50} values were adjusted to account for the fact that four molecules of ALA are required for the formation of the active species protoporphyrin IX. [g]From ref 64.

Although the excellent phototoxicity of these Ir(III) complexes, under both OPE and TPE conditions, could be largely attributed to their high $^1O_2$ yield, we have also tested other possible antitumor mechanisms related to DNA binding. The DNA-binding properties of **Ir1**−**Ir4** have been studied by absorption spectral titration, DNA thermal denaturation, and DNA viscosity measurements. With increasing amounts of CT-DNA, the absorption spectra of **Ir1**−**Ir4** showed slight changes in both absorbance (hypochromic effect less than 5%) and wavelength of absorption peaks (red shift less than 3 nm), as displayed in Figure S8. Negligible differences have been found in the melting point of DNA (T_m) in the absence and presence of Ir(III) complexes ([DNA]/[Ir] = 10/1), as illustrated in Figure S9. The viscosity of DNA also showed slight changes in the presence of Ir(III) complexes in the tested concentration range (Figure S10). All of these results suggested that **Ir1**−**Ir4** have very low DNA affinity. Therefore, they are unlikely to have a significant inhibitory effect on DNA-related enzymes. This may explain why these compounds showed very low dark toxicity and their selectivity for mitochondria instead of the nucleus, where the DNA content is obviously high.

CONCLUSIONS

Since TLD1433 has entered a human clinical trial, more attention should be paid to the pharmaceutical issue in the research of PDT agents, in addition to the pursuit of high activity. In this study, four cyclometalated Ir(III) complexes that can specifically accumulate in mitochondria have been designed and prepared by an optimized synthetic route with apparently higher yield, productivity, and efficiency in comparison to the traditional methods. With the help of a spectroscopic study and DFT/TDDFT quantum chemistry theoretical calculations, their ground state and excited singlet and triplet state properties have been understood in detail. **Ir1** and **Ir3** have high $^1O_2$ production quantum yields, impressive TP absorption properties, and a low dark cytotoxicity. Importantly, they could induce cell apoptosis upon TP irradiation with very high PIs in comparison to similar complexes. These Ir(III) complexes, especially **Ir3**, hold great promise as TP mitochondrial dye and PDT agents.

Overall, in this study, TP-PDT agents with high antitumor activity and PI were successfully designed by the combination of a substituent group which can amplify ROS and an Ir(III) complex with good TP-PDT properties. The results suggest that the complexes have enormous potential for application as a mitochondrion-specific dye in cell biology as well as a photosensitizer for TP-PDT in medicine. Studies using **Ir3** as in vivo TP-PDT agents and further modification of the ppy ligands to improve the PDT activity and PI are currently underway.

ASSOCIATED CONTENT

Supporting Information

The Supporting Information is available free of charge at https://pubs.acs.org/doi/10.1021/acs.inorgchem.0c01509.

Optimized structures and frontier molecular orbitals, simulated and experimental electronic absorption spectra, cyclic voltammetry, emission spectra in aqueous solution, time-dependent changes in absorption spectra of DPBF in the presence of Ir(III) complexes, Pearson's correlation coefficient (R) analysis (PCCA) between Ir(III) complexes and MTG by CLSM on human cancer

https://dx.doi.org/10.1021/acs.inorgchem.0c01509
Inorg. Chem. XXXX, XXX, XXX−XXX

cells A549, Z-stack images of A549 stained by Ir(III) complexes, DNA-binding experiments, and experimental and computational absorption spectral data and Cartesian coordinates of the optimized structures of Ir(III) complexes for S0, S1, and T1 states (PDF)

AUTHOR INFORMATION

Corresponding Authors

Dandan Liu − *School of Pharmaceutical Sciences and Yunnan Key Laboratory of Pharmacology for Natural Products, Kunming Medical University, Kunming 650500, Yunnan, People's Republic of China*; Email: 709249906@qq.com

Feng Gao − *Key Laboratory of Medicinal Chemistry for Natural Resource, Ministry of Education, Yunnan Research & Development Center for Natural Products, School of Chemical Science and Technology, Yunnan University, Kunming 650091, Yunnan, People's Republic of China*; orcid.org/0000-0001-7490-4887; Email: gaofeng@ynu.edu.cn

Authors

Xu-Dan Bi − *Key Laboratory of Medicinal Chemistry for Natural Resource, Ministry of Education, Yunnan Research & Development Center for Natural Products, School of Chemical Science and Technology, Yunnan University, Kunming 650091, Yunnan, People's Republic of China*

Rong Yang − *Key Laboratory of Medicinal Chemistry for Natural Resource, Ministry of Education, Yunnan Research & Development Center for Natural Products, School of Chemical Science and Technology, Yunnan University, Kunming 650091, Yunnan, People's Republic of China*

Yue-Chen Zhou − *Key Laboratory of Medicinal Chemistry for Natural Resource, Ministry of Education, Yunnan Research & Development Center for Natural Products, School of Chemical Science and Technology, Yunnan University, Kunming 650091, Yunnan, People's Republic of China*

Daomei Chen − *National Center for International Research on Photoelectric and Energy Materials, School of Materials and Energy, Yunnan University, Kunming 650091, People's Republic of China*

Guo-Kui Li − *Key Laboratory of Medicinal Chemistry for Natural Resource, Ministry of Education, Yunnan Research & Development Center for Natural Products, School of Chemical Science and Technology, Yunnan University, Kunming 650091, Yunnan, People's Republic of China*

Yuan-Xiao Guo − *Key Laboratory of Medicinal Chemistry for Natural Resource, Ministry of Education, Yunnan Research & Development Center for Natural Products, School of Chemical Science and Technology, Yunnan University, Kunming 650091, Yunnan, People's Republic of China*

Meng-Fan Wang − *Key Laboratory of Medicinal Chemistry for Natural Resource, Ministry of Education, Yunnan Research & Development Center for Natural Products, School of Chemical Science and Technology, Yunnan University, Kunming 650091, Yunnan, People's Republic of China*

Complete contact information is available at: https://pubs.acs.org/10.1021/acs.inorgchem.0c01509

Notes

The authors declare no competing financial interest.

ACKNOWLEDGMENTS

This work was supported by National Natural Science Foundation of China (21662039, 21907044), Yunnan Provincial Science and Technology Department (2018FB022, 2019FB124), Ten Thousand Talents Project of Yunnan Province (YNWR-QNBJ-2018-057), and the Program for Changjiang Scholars and Innovative Research Team in University (IRT17R94). F.G. thanks the High Performance Computing Center of Yunnan University for computational support. D.L. acknowledges the support of grants from the Hundred Talent Program of Kunming Medical University.

REFERENCES

(1) *Photodynamic Therapy: Basic Principles and Clinical Applications*; Henderson, B. W., Dougherty, T. J., Eds.; CRC Press: 1992.

(2) *Photodynamic Medicine: From Bench to Clinic*, 1st ed.; Kostron, H., Hasan, T., Eds.; Royal Society of Chemistry: Cambridge, U.K., 2016.

(3) van Straten, D.; Mashayekhi, V.; de Bruijn, H.; Oliveira, S.; Robinson, D. Oncologic Photodynamic Therapy: Basic Principles, Current Clinical Status and Future Directions. *Cancers* **2017**, *9*, 19.

(4) Deng, K.; Li, C.; Huang, S.; Xing, B.; Jin, D.; Zeng, Q.; Hou, Z.; Lin, J. Recent Progress in Near Infrared Light Triggered Photodynamic Therapy. *Small* **2017**, *13* (44), 1702299.

(5) Ai, X.; Mu, J.; Xing, B. Recent Advances of Light-Mediated Theranostics. *Theranostics* **2016**, *6* (13), 2439−2457.

(6) Ethirajan, M.; Chen, Y.; Joshi, P.; Pandey, R. K. The role of porphyrin chemistry in tumor imaging and photodynamic therapy. *Chem. Soc. Rev.* **2011**, *40* (1), 340−362.

(7) Tian, J.; Ding, L.; Xu, H. J.; Shen, Z.; Ju, H.; Jia, L.; Bao, L.; Yu, J. S. Cell-specific and pH-activatable rubyrin-loaded nanoparticles for highly selective near-infrared photodynamic therapy against cancer. *J. Am. Chem. Soc.* **2013**, *135* (50), 18850−18858.

(8) Chen, G.; Qiu, H.; Prasad, P. N.; Chen, X. Upconversion nanoparticles: design, nanochemistry, and applications in theranostics. *Chem. Rev.* **2014**, *114* (10), 5161−5214.

(9) Dong, H.; Du, S. R.; Zheng, X. Y.; Lyu, G. M.; Sun, L. D.; Li, L. D.; Zhang, P. Z.; Zhang, C.; Yan, C. H. Lanthanide Nanoparticles: From Design toward Bioimaging and Therapy. *Chem. Rev.* **2015**, *115* (19), 10725−10815.

(10) Shen, Y.; Shuhendler, A. J.; Ye, D.; Xu, J. J.; Chen, H. Y. Two-photon excitation nanoparticles for photodynamic therapy. *Chem. Soc. Rev.* **2016**, *45* (24), 6725−6741.

(11) Ogilby, P. R. Singlet oxygen: there is indeed something new under the sun. *Chem. Soc. Rev.* **2010**, *39* (8), 3181−3209.

(12) Zamora, A.; Vigueras, G.; Rodriguez, V.; Santana, M. D.; Ruiz, J. Cyclometalated iridium(III) luminescent complexes in therapy and phototherapy. *Coord. Chem. Rev.* **2018**, *360*, 34−76.

(13) Collins, H. A.; Khurana, M.; Moriyama, E. H.; Mariampillai, A.; Dahlstedt, E.; Balaz, M.; Kuimova, M. K.; Drobizhev, M.; Yang, V. X. D.; Phillips, D.; Rebane, A.; Wilson, B. C.; Anderson, H. L. Blood-vessel closure using photosensitizers engineered for two-photon excitation. *Nat. Photonics* **2008**, *2* (7), 420−424.

(14) Heinemann, F.; Karges, J.; Gasser, G. Critical Overview of the Use of Ru(II) Polypyridyl Complexes as Photosensitizers in One-Photon and Two-Photon Photodynamic Therapy. *Acc. Chem. Res.* **2017**, *50* (11), 2727−2736.

(15) Liu, J. P.; Zhang, C.; Rees, T. W.; Ke, L. B.; Ji, L. N.; Chao, H. Harnessing ruthenium(II) as photodynamic agents: Encouraging advances in cancer therapy. *Coord. Chem. Rev.* **2018**, *363*, 17−28.

(16) Poynton, F. E.; Bright, S. A.; Blasco, S.; Williams, D. C.; Kelly, J. M.; Gunnlaugsson, T. The development of ruthenium(II) polypyridyl complexes and conjugates for in vitro cellular and in vivo applications. *Chem. Soc. Rev.* **2017**, *46* (24), 7706−7756.

(17) Reessing, F.; Szymanski, W. Beyond Photodynamic Therapy: Light-Activated Cancer Chemotherapy. *Curr. Med. Chem.* **2018**, *24* (42), 4905−4950.

https://dx.doi.org/10.1021/acs.inorgchem.0c01509
Inorg. Chem. XXXX, XXX, XXX−XXX

(18) Josefsen, L. B.; Boyle, R. W. Photodynamic Therapy and the Development of Metal-Based hotosensitisers. *Met.-Based Drugs* **2008**, *2008*, 1−23.
(19) Cho, S.; You, Y.; Nam, W. Lysosome-specific one-photon fluorescence staining and two-photon singlet oxygen generation by molecular dyad. *RSC Adv.* **2014**, *4* (33), 16913−16916.
(20) Boca, S. C.; Four, M.; Bonne, A.; van der Sanden, B.; Astilean, S.; Baldeck, P. L.; Lemercier, G. An ethylene-glycol decorated ruthenium(ii) complex for two-photon photodynamic therapy. *Chem. Commun.* **2009**, No. 30, 4590−4592.
(21) Boreham, E. M.; Jones, L.; Swinburne, A. N.; Blanchard-Desce, M.; Hugues, V.; Terryn, C.; Miomandre, F.; Lemercier, G.; Natrajan, L. S. A cyclometallated fluorenyl Ir(iii) complex as a potential sensitiser for two-photon excited photodynamic therapy (2PE-PDT). *Dalton Trans.* **2015**, *44* (36), 16127−16135.
(22) Bolze, F.; Jenni, S.; Sour, A.; Heitz, V. Molecular photosensitisers for two-photon photodynamic therapy. *Chem. Commun.* **2017**, *53* (96), 12857−12877.
(23) Day, A. H.; Übler, M. H.; Best, H. L.; Lloyd-Evans, E.; Mart, R. J.; Fallis, I. A.; Allemann, R. K.; Al-Wattar, E. A. H.; Keymer, N. I.; Buurma, N. J.; Pope, S. J. A. Targeted cell imaging properties of a deep red luminescent iridium(iii) complex conjugated with a c-Myc signal peptide. *Chem. Sci.* **2020**, *11* (6), 1599−1606.
(24) Colombo, A.; Fontani, M.; Dragonetti, C.; Roberto, D.; Williams, J. A. G.; Scotto di Perrotolo, R.; Casagrande, F.; Barozzi, S.; Polo, S. A Highly Luminescent Tetrahydrocurcumin IrIII Complex with Remarkable Photoactivated Anticancer Activity. *Chem. - Eur. J.* **2019**, *25* (33), 7948−7952.
(25) Wang, W.; Lu, L.; Wu, K. J.; Liu, J.; Leung, C. H.; Wong, C. Y.; Ma, D. L. Long-lived iridium(III) complexes as luminescent probes for the detection of periodate in living cells. *Sens. Actuators, B* **2019**, *288*, 392−398.
(26) Caporale, C.; Massi, M. Cyclometalated iridium(III) complexes for life science. *Coord. Chem. Rev.* **2018**, *363*, 71−91.
(27) Shaikh, S.; Wang, Y.; ur Rehman, F.; Jiang, H.; Wang, X. Phosphorescent Ir(III) complexes as cellular staining agents for biomedical molecular imaging. *Coord. Chem. Rev.* **2020**, *416*, 213344.
(28) Ho, P. Y.; Ho, C. L.; Wong, W. Y. Recent advances of iridium(III) metallophosphors for health-related applications. *Coord. Chem. Rev.* **2020**, *413*, 213267.
(29) Huang, H.; Banerjee, S.; Sadler, P. J. Recent Advances in the Design of Targeted Iridium(III) Photosensitizers for Photodynamic Therapy. *ChemBioChem* **2018**, *19* (15), 1574−1589.
(30) Zhang, T.; Lan, R.; Chan, C.-F.; Law, G.-L.; Wong, W.-K.; Wong, K.-L. In vivo selective cancer-tracking gadolinium eradicator as new-generation photodynamic therapy agent. *Proc. Natl. Acad. Sci. U. S. A.* **2014**, *111* (51), E5492.
(31) Galland, M.; Le Bahers, T.; Banyasz, A.; Lascoux, N.; Duperray, A.; Grichine, A.; Tripier, R.; Guyot, Y.; Maynadier, M.; Nguyen, C.; Gary-Bobo, M.; Andraud, C.; Monnereau, C.; Maury, O. A "Multi-Heavy-Atom" Approach toward Biphotonic Photosensitizers with Improved Singlet-Oxygen Generation Properties. *Chem. - Eur. J.* **2019**, *25* (38), 9026−9034.
(32) Monro, S.; Colón, K. L.; Yin, H.; Roque, J.; Konda, P.; Gujar, S.; Thummel, R. P.; Lilge, L.; Cameron, C. G.; McFarland, S. A. Transition Metal Complexes and Photodynamic Therapy from a Tumor-Centered Approach: Challenges, Opportunities, and Highlights from the Development of TLD1433. *Chem. Rev.* **2019**, *119* (2), 797−828.
(33) Hamblin, M. R.; Mroz, P. *Advances in Photodynamic Therapy: Basic, Translational, and Clinical; Engineering in Medicine and Biology*; Artech House: Norwood, MA, 2008.
(34) Ka, H.; Park, H.-J.; Jung, H.-J.; Choi, J.-W.; Cho, K.-S.; Ha, J.; Lee, K.-T. Cinnamaldehyde induces apoptosis by ROS-mediated mitochondrial permeability transition in human promyelocytic leukemia HL-60 cells. *Cancer Lett.* **2003**, *196* (2), 143−152.
(35) Ma, S.; Song, W.; Xu, Y.; Si, X.; Lv, S.; Zhang, Y.; Tang, Z.; Chen, X. Rationally Designed Polymer Conjugate for Tumor-Specific Amplification of Oxidative Stress and Boosting Antitumor Immunity. *Nano Lett.* **2020**, *20* (4), 2514−2521.
(36) Nakamaru, K. Synthesis, Luminescence Quantum Yields, and Lifetimes of Trischelated Ruthenium(Ii) Mixed-Ligand Complexes Including 3,3′-Dimethyl-2,2'-Bipyridyl. *Bull. Chem. Soc. Jpn.* **1982**, *55* (9), 2697−2705.
(37) Xu, W. J.; Liu, S. J.; Zhao, X.; Zhao, N.; Liu, Z. Q.; Xu, H.; Liang, H.; Zhao, Q.; Yu, X. Q.; Huang, W. *Chem. - Eur. J.* **2013**, *19*, 621−629.
(38) Yamada, M.; Tanaka, Y.; Yoshimoto, Y.; Kuroda, S.; Shimao, I. Synthesis and Properties of Diamino-Substituted Dipyrido[3,2-a 2',3′-C]Phenazine. *Bull. Chem. Soc. Jpn.* **1992**, *65* (4), 1006−1011.
(39) Guo, W. L.; Ding, H.; Gu, C. Y.; Liu, Y. H.; Jiang, X. C.; Su, B.; Shao, Y. H. Potential-Resolved Multicolor Electrochemiluminescence for Multiplex Immunoassay in a Single Sample. *J. Am. Chem. Soc.* **2018**, *140* (46), 15904−15915.
(40) Li, L. P.; Ye, B. H. Efficient Generation of Singlet Oxygen and Photooxidation of Sulfide into Sulfoxide via Tuning the Ancillary of Bicyclometalated Iridium(III) Complexes. *Inorg. Chem.* **2019**, *58* (12), 7775−7784.
(41) Frisch, M. J.; Trucks, G. W.; Schlegel, H. B.; Scuseria, G. E.; Robb, M. A.; Cheeseman, J. R.; Scalmani, G.; Barone, V.; Mennucci, B.; Peterson, G. A.; Nakatsuji, H.; Caricato, M.; Li, X.; Hratchian, H. P.; Izmaylov, A. F.; Bloino, J.; Zheng, G.; Sonnenberg, J. L.; Hada, M.; Ehara, M.; Toyota, K.; Fukuda, R.; Hasegawa, J.; Ishida, M.; Nakajima, T.; Honda, Y.; Kitao, O.; Nakai, H.; Vreven, T.; Montgomery, J. A., Jr.; Peralta, J. E.; Ogliaro, F.; Bearpark, M.; Heyd, J. J.; Brothers, E.; Kudin, K. N.; Staroverov, V. N.; Kobayashi, R.; Normand, J.; Raghavachari, K.; Rendell, A.; Burant, J. C.; Iyengar, S. S.; Tomasi, J.; Cossi, M.; Rega, N.; Millam, J. M.; Klene, M.; Knox, J. E.; Cross, J. B.; Bakken, V.; Adamo, C.; Jaramillo, J.; Gomperts, R.; Stratmann, R. E.; Yazyev, O.; Austin, A. J.; Cammi, R.; Pomelli, C.; Ochterski, J. W.; Martin, R. L.; Morokuma, K.; Zakrzewski, V. G.; Voth, G. A.; Salvador, P.; Dannenberg, J. J.; Dapprich, S.; Daniels, A. D.; Farkas, O.; Foresman, J. B.; Ortiz, J. V.; Cioslowski, J.; Fox, D. J. *Gaussian 09, rev. B.1*; Gaussian, Inc.: Wallingford, CT, 2009.
(42) Hay, P. J.; Wadt, W. R. Ab initio effective core potentials for molecular calculations. Potentials for K to Au including the outermost core orbitals. *J. Chem. Phys.* **1985**, *82* (1), 299−310.
(43) Barone, V.; Cossi, M.; Tomasi, J. Geometry optimization of molecular structures in solution by the polarizable continuum model. *J. Comput. Chem.* **1998**, *19* (4), 404−417.
(44) Martin, R. L. Natural transition orbitals. *J. Chem. Phys.* **2003**, *118* (11), 4775−4777.
(45) Badaeva, E.; Albert, V. V.; Kilina, S.; Koposov, A.; Sykora, M.; Tretiak, S. Effect of deprotonation on absorption and emission spectra of Ru(II)-bpy complexes functionalized with carboxyl groups. *Phys. Chem. Chem. Phys.* **2010**, *12* (31), 8902−13.
(46) Liu, R.; Dandu, N.; Chen, J.; Li, Y.; Li, Z.; Liu, S.; Wang, C.; Kilina, S.; Kohler, B.; Sun, W. Influence of Different Diimine (N^N) Ligands on the Photophysics and Reverse Saturable Absorption of Heteroleptic Cationic Iridium(III) Complexes Bearing Cyclometalating 2-{3-[7-(Benzothiazol-2-yl)fluoren-2-yl]phenyl}pyridine (C^N) Ligands. *J. Phys. Chem. C* **2014**, *118* (40), 23233−23246.
(47) Gao, F.; Chen, X.; Wang, J. Q.; Chen, Y.; Chao, H.; Ji, L. N. In vitro transcription inhibition by ruthenium(II) polypyridyl complexes with electropositive ancillary ligands. *Inorg. Chem.* **2009**, *48* (13), 5599−5601.
(48) Schneider, C. A.; Rasband, W. S.; Eliceiri, K. W. NIH Image to ImageJ: 25 years of image analysis. *Nat. Methods* **2012**, *9* (7), 671−675.
(49) Sun, W.; Pei, C.; Lu, T.; Cui, P.; Li, Z.; McCleese, C.; Fang, Y.; Kilina, S.; Song, Y.; Burda, C. Reverse saturable absorbing cationic iridium(iii) complexes bearing the 2-(2-quinolinyl)quinoxaline ligand: effects of different cyclometalating ligands on linear and nonlinear absorption. *J. Mater. Chem. C* **2016**, *4* (22), 5059−5072.
(50) Zhao, Q.; Liu, S.; Shi, M.; Wang, C.; Yu, M.; Li, L.; Li, F.; Yi, T.; Huang, C. Series of New Cationic Iridium(III) Complexes with Tunable Emission Wavelength and Excited State Properties:

https://dx.doi.org/10.1021/acs.inorgchem.0c01509
Inorg. Chem. XXXX, XXX, XXX−XXX

Structures, Theoretical Calculations, and Photophysical and Electrochemical Properties. *Inorg. Chem.* **2006**, *45* (16), 6152−6160.
(51) Zhang, K. Y.; Li, S. P.; Zhu, N.; Or, I. W.; Cheung, M. S.; Lam, Y. W.; Lo, K. K. Structure, photophysical and electrochemical properties, biomolecular interactions, and intracellular uptake of luminescent cyclometalated iridium(III) dipyridoquinoxaline complexes. *Inorg. Chem.* **2010**, *49* (5), 2530−40.
(52) Liu, B.; Lystrom, L.; Kilina, S.; Sun, W. Tuning the Ground State and Excited State Properties of Monocationic Iridium(III) Complexes by Varying the Site of Benzannulation on Diimine Ligand. *Inorg. Chem.* **2017**, *56* (9), 5361−5370.
(53) Liu, B.; Lystrom, L.; Kilina, S.; Sun, W. Effects of Varying the Benzannulation Site and pi Conjugation of the Cyclometalating Ligand on the Photophysics and Reverse Saturable Absorption of Monocationic Iridium(III) Complexes. *Inorg. Chem.* **2019**, *58* (1), 476−488.
(54) Lowry, M. S.; Goldsmith, J. I.; Slinker, J. D.; Rohl, R.; Pascal, R. A.; Malliaras, G. G.; Bernhard, S. Single-Layer Electroluminescent Devices and Photoinduced Hydrogen Production from an Ionic Iridium(III) Complex. *Chem. Mater.* **2005**, *17* (23), 5712−5719.
(55) Nazeeruddin, M. K.; Wegh, R. T.; Zhou, Z.; Klein, C.; Wang, Q.; De Angelis, F.; Fantacci, S.; Grätzel, M. Efficient Green-Blue-Light-Emitting Cationic Iridium Complex for Light-Emitting Electrochemical Cells. *Inorg. Chem.* **2006**, *45* (23), 9245−9250.
(56) Zhao, J.; Wu, W.; Sun, J.; Guo, S. Triplet photosensitizers: from molecular design to applications. *Chem. Soc. Rev.* **2013**, *42* (12), 5323−5351.
(57) Zeng, X.; Tavasli, M.; Perepichka, I. F.; Batsanov, A. S.; Bryce, M. R.; Chiang, C.-J.; Rothe, C.; Monkman, A. P. Cationic Bis-cyclometallated Iridium(III) Phenanthroline Complexes with Pendant Fluorenyl Substituents: Synthesis, Redox, Photophysical Properties and Light-Emitting Cells. *Chem. - Eur. J.* **2008**, *14* (3), 933−943.
(58) Li, Y.; Dandu, N.; Liu, R.; Kilina, S.; Sun, W. Synthesis and photophysics of reverse saturable absorbing heteroleptic iridium(iii) complexes bearing 2-(7-R-fluoren-2′-yl)pyridine ligands. *Dalton Trans.* **2014**, *43* (4), 1724−1735.
(59) Wang, L.; Yin, H.; Cui, P.; Hetu, M.; Wang, C.; Monro, S.; Schaller, R. D.; Cameron, C. G.; Liu, B.; Kilina, S.; McFarland, S. A.; Sun, W. Near-infrared-emitting heteroleptic cationic iridium complexes derived from 2,3-diphenylbenzo[g]quinoxaline as in vitro theranostic photodynamic therapy agents. *Dalton Trans.* **2017**, *46* (25), 8091−8103.
(60) Jin, C.; Liu, J.; Chen, Y.; Zeng, L.; Guan, R.; Ouyang, C.; Ji, L.; Chao, H. Cyclometalated Iridium(III) Complexes as Two-Photon Phosphorescent Probes for Specific Mitochondrial Dynamics Tracking in Living Cells. *Chem. - Eur. J.* **2015**, *21* (34), 12000−12010.
(61) Furuta, T.; Wang, S. S.-H.; Dantzker, J. L.; Dore, T. M.; Bybee, W. J.; Callaway, E. M.; Denk, W.; Tsien, R. Y. Brominated 7-hydroxycoumarin-4-ylmethyls: Photolabile protecting groups with biologically useful cross-sections for two photon photolysis. *Proc. Natl. Acad. Sci. U. S. A.* **1999**, *96*, 1193−1200.
(62) Lv, W.; Zhang, Z.; Zhang, K. Y.; Yang, H.; Liu, S.; Xu, A.; Guo, S.; Zhao, Q.; Huang, W. A Mitochondria-Targeted Photosensitizer Showing Improved Photodynamic Therapy Effects Under Hypoxia. *Angew. Chem., Int. Ed.* **2016**, *55* (34), 9947−9951.
(63) Bevernaegie, R.; Doix, B.; Bastien, E.; Diman, A.; Decottignies, A.; Feron, O.; Elias, B. Exploring the Phototoxicity of Hypoxic Active Iridium(III)-Based Sensitizers in 3D Tumor Spheroids. *J. Am. Chem. Soc.* **2019**, *141* (46), 18486−18491.
(64) Yuan, B.; Liu, J.; Guan, R.; Jin, C.; Ji, L.; Chao, H. Endoplasmic reticulum targeted cyclometalated iridium(III) complexes as efficient photodynamic therapy photosensitizers. *Dalton Trans.* **2019**, *48* (19), 6408−6415.
(65) Vaillant, O.; El Cheikh, K.; Warther, D.; Brevet, D.; Maynadier, M.; Bouffard, E.; Salgues, F.; Jeanjean, A.; Puche, P.; Mazerolles, C.; Maillard, P.; Mongin, O.; Blanchard-Desce, M.; Raehm, L.; Rebillard, X.; Durand, J. O.; Gary-Bobo, M.; Morere, A.; Garcia, M. Mannose-6-phosphate receptor: a target for theranostics of prostate cancer. *Angew. Chem., Int. Ed.* **2015**, *54* (20), 5952−5956.

https://dx.doi.org/10.1021/acs.inorgchem.0c01509
Inorg. Chem. XXXX, XXX, XXX−XXX